On the structure of wave-particle interactions and nonlinear Alfvénic fluctuation dynamics

X. Wang[1], S. Briguglio[2], M. Schneller[3], Ph. Lauber[1], V. Fusco[2], C. Di Troia[2], G. Fogaccia[2], G. Vlad[2] and F. Zonca[2,4]

[1]Max-Planck-Institut fur Plasmaphysik, Boltzmannstrasse 2, Garching D-85748, Germany
[2]C.R. ENEA Frascati - C.P. 65, 00044 Frascati, Italy
[3]Princeton Plasma Physics Laboratory, Princeton, NJ 08543, USA
[4]Institute for Fusion Theory and Simulation and Department of Physics, Zhejiang University Hangzhou 310027, Peoples Republic of China

Corresponding Author: xin.wang@ipp.mpg.de

Abstract:
Nonlinear dynamics, such as saturation and frequency chirping of Alfvénic fluctuations driven by energetic particles are investigated by means of the nonlinear hybrid magnetohydrodynamics gyrokinetic code (XHMGC). Saturation mechanism due to resonance detuning and/or radial decoupling are discussed. It will be shown that saturation field level exhibits a quadratic scaling with the growth rate, in the former case; a linear scaling, in the latter case. The dominance of one or the other mechanism depends on the linear properties of the mode (in particular, the growth rate, the spatial structure and the radial dependence of the resonance frequency). For the frequency chirping of EPMs, phase locking has been proposed, within "fishbone" paradigm, to describe such chirping: the resonance condition with linearly resonant particles is maintained, while particles are radially displaced, through a continuous modification of the mode frequency. Meanwhile an additional scenario is possible: mode radial localization and frequency appear to be locked to the shear Alfvén continuum; once the linear resonance population has exhausted its driving capability (because of local flattening of the phase-space distribution function), the mode is shifted to non-exhausted regions of the phase space. The effect is a succession of resonant excitations from different phase-space regions (each characterized by its own nonlinear evolution time), rather than mode adjustment to the evolution of the linearly-resonant particles. Both mechanisms demonstrate that the frequency chirping is due to the procedure of maximising the wave-particle power exchange.

1 Introduction

Shear-Alfvén modes can be driven unstable by energetic particles (EPs) produced by additional heating or nuclear fusion reactions. Alfvénic fluctuations can, in turn, be derimental to EP confinement and lead large EP losses. Understanding the properties of

EP confinement largely depends on the insights into Alfvén mode dynamics, with regard to both the linear stability properties [1]; and the nonlinear dynamics, which have recently attracted significant interest both on theoretical and numerical analysis sides. In general, the nonlinear dynamics of Alfvén eigenmodes (AEs) can be classified into two major categories: mode-mode coupling and nonlinear wave-particle interactions. Although the former can play a crucial role in multi-scale dynamics of burning plasmas [2], we will focus, in the current work, on the latter category, motivated by the relevance of the resonant drive on the Alfvénic fluctuation spectrum in fusion devices. Two opposite limits of nonlinear wave-particle dynamics have been widely investigated: weakly driven AEs (e.g. Toroidal Alfvén eigenmodes (TAEs) [3]) close to marginal stability, for which mode saturation is due to phase mixing of resonant particles trapped in the potential well of the wave and the radial excursion of EPs is very limited with formation of phase-space holes and clumps and adiabatic frequency chirping due to resonant frequencies following hole and clump propagation [4]; strongly driven Energetic Particle Modes (EPMs) [5], for which saturation is due to macroscopic distortion of the EP pressure profile and the interplay between mode structure and resonant particles is crucial, since the radial excursion of resonant particles is comparable with the length scale of equilibrium or fluctuation induced non-uniformities [6]. The analysis of the intermediate situation (moderately unstable modes) has not yet been analyzed in proper detail. In our work, nonlinear dynamics, such as amplitude saturation and frequency chirping, in such intermediate regime are investigated by means of the nonlinear hybrid magnetohydrodynamics gyrokinetic code (XHMGC) [7, 8].

2 Saturation mechanism

Saturation mechanism due to resonance detuning and/or radial decoupling are discussed. The saturation field level exhibits a quadratic scaling with the growth rate, in the former case; a linear scaling, in the latter case. How the dominance of one or the other mechanism depends on the linear properties of the mode (in particular, the growth rate, the spatial structure and the radial dependence of the resonance frequency). These fundamental results/scaling are crucial for any reduced/simplified EP transport model which is needed for fast and flexible predictive tools to be developed in the future.

Resonance detuning and radial decoupling – The importance of plasma non-uniformity has been pointed out by Refs. [1, 6], in the frame of the so-called "fishbone" paradigm. The basic point is that, for increasing drive and, hence, mode amplitude, particle orbits become able to explore the finite radial-width of the fields. At the same time, the resonance condition is satisfied, in this limit, in a wider radial region (whose width scales with the mode growth rate). The spatial region where the mode-particle power exchange can take place becomes than limited by the mode width rather than the resonance width. Saturation occurs when the flattening region of the resonant particle density profile extends by the whole region in which the mode-particle power exchange can occur. Such region will be limited both by the finite mode width and the finite resonance width. This is represented in Fig.1. The resonance width is determined by the condition $|\omega - \omega_{\rm res}| \leq \gamma_L$; it then increases with the linear growth rate γ_L. Two opposite regimes are represented

in Fig.1(left) and (right), respectively. In the former ("resonance detuning" regime), the most stringent constraint on power exchange is set by the resonance width; in the latter ("radial decoupling" regime), it is set by the mode width. The transition from the resonance detuning regime to the radial decoupling one occurs, *ceteris paribus*, as larger drive, narrower modes and/or flatter resonance frequency profiles are considered.

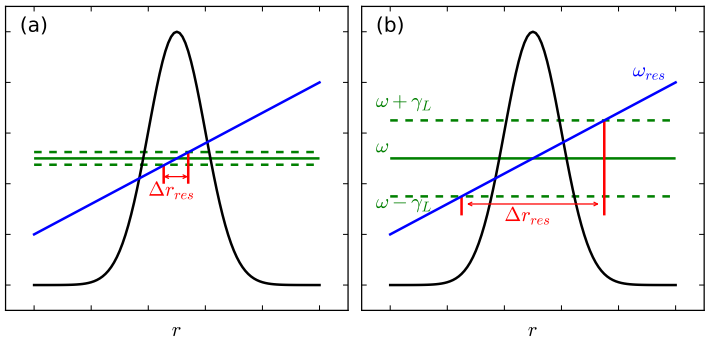

FIG. 1: Model comparison between the radial mode structure (black line) and the radial resonance profile (blue line). The green solid line indicates the mode frequency ω, while dashed lines correspond to $\omega \pm \gamma_L$. The resonance width Δr_{res} is approximately defined as the width of the region where the condition $|\omega - \omega_{\rm res}| \leq \gamma_L$ is satisfied. Frame (a) represents a situation in which the mode structure is larger than the resonance width; frame (b), the opposite situation.

XHMGC simulation results – In our work, the simulations of BAE modes driven unstable by purely circulating EPs are performed for analysing the saturation mechanism. A tokamak equilibrium is considered, characterized by aspect ratio $R_0/a = 10$ and safety factor $q = q_0 + (q_a - q_0)(r/a)^2$, with $q_0 = 1.9$ and $q_a = 2.3$. The results of simulations related to modes characterised, respectively, by toroidal numbers $n = 2$, 3 and 4, are reported. Different toroidal numbers correspond to different shapes of the shear-Alfvén continuum; then, both mode structure and mode frequency change. The normalized mode structure of the scalar potential and the mode frequency spectrum are shown in Fig. 2 for each n. The unstable modes are all located near the shear-Alfvén continuum accumulation point for each n. Mode frequencies are very similar for co-passing fast ion driven modes and counter-passing ones for all n values. They increase as the toroidal mode number increases. The mode structure is narrower for larger toroidal mode number n.

The results of the mode saturation amplitude varying as the growth rate obtained at different values of n_H/n_i or different toroidal mode numbers are reported in Fig. 3, for modes driven by co-passing fast ions (left) and counter-passing ones (right). A clear transition from quadratic to linear scaling is observed in the counter-passing fast ion case, for all the values of the toroidal mode number n. The growth rate value at which the transition occurs slightly increases with increasing n. At the same time, the corresponding mode saturation amplitude decreases. The situation is less defined in the co-passing fast ion case. In particular, no transition is observed for $n = 2$, with the mode saturation amplitude scaling linearly over the whole considered range of n_H/n_i. For $n = 3$, although

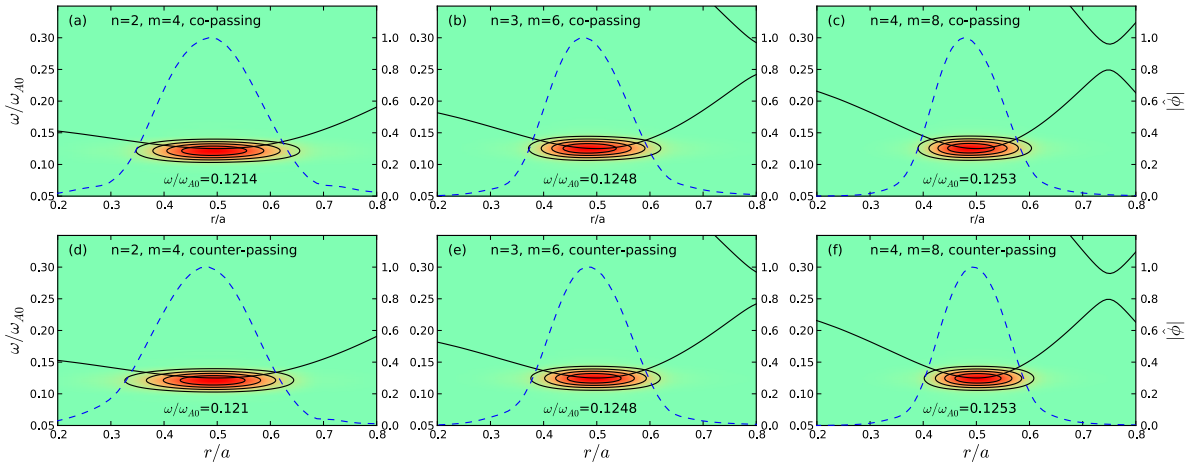

FIG. 2: Energy spectrum for the scalar potential, in the (r, ω) plane, for the BAE driven by fast ions, as obtained from XHMGC simulations for different choices of the toroidal mode number n. The normalised radial structure of the dominant harmonic for the scalar potential is also reported for each case (dashed lines). Top frames refer to modes driven by co-passing fast ions; bottom frames, to modes driven by counter-passing fast ions. Here ω_{A0} is the one-axis Alfvén speed.

a quadratic scaling can not be revealed, a deviation from the linear scaling is observed when moving from the stronger to the weaker cases. It is still true that the transition growth rate value increases with n (for $n = 2$ and $n = 3$ we can only set upper limits to such value, with the limit relative to the $n = 2$ case being surely lower than that pertaining to the $n = 3$ case). Nothing can be said, instead, about the variation of the transition values of the mode saturation amplitude.

It has been demonstrated [9] that mode saturation occurs as the flattening of the resonant particle distribution function profile (which represent the free-energy source for mode instability) extends over the whole region where the mode-particle interaction can take place. This region is limited both by the finite radial structure of the mode ($\Delta r_{\rm mode}$) and the finite radial extension where the resonance condition, $|\omega - \omega_{\rm res}(r)| \lesssim \gamma_L$, is satisfied ($\Delta r_{\rm res}$). Saturation will be reached as

$$A^{\rm sat}/\gamma_L \sim \min[\gamma_L/|S|, \Delta r_{\rm mode}]. \tag{1}$$

Taking into account that the mode width exhibits a negligible dependence on the growth rate, we see that the quadratic scaling for the mode saturation amplitude is obtained when the most stringent constraint is represented by the resonance width (resonance detuning regime); the linear scaling, when it is given by the finite mode width (radial decoupling regime). Transition from the former to the latter regime is expected for

$$\gamma_{L\,\rm tr} \sim |S| \Delta r_{\rm mode}, \tag{2}$$

with a saturation amplitude

$$A^{\rm sat}_{\rm tr} \sim |S| \Delta r^2_{\rm mode}. \tag{3}$$

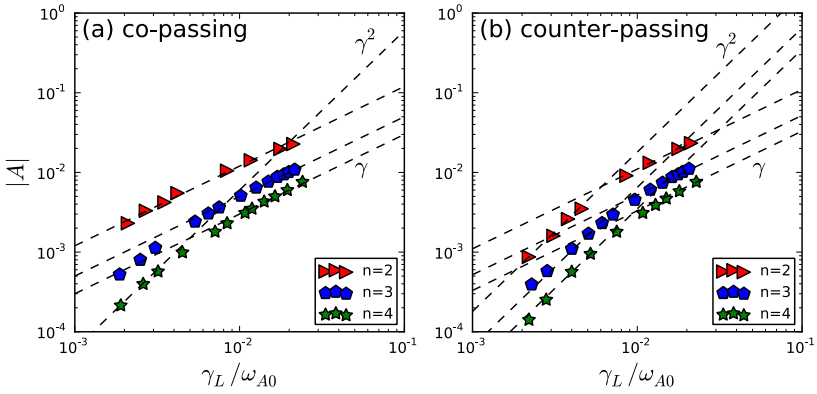

FIG. 3: Scaling of saturation amplitude of scalar potential versus normalized linear growth rate for different toroidal numbers, for co-passing (left) and counter-passing (right) fast ions. The reference quadratic and linear γ_L scaling are also shown.

In the present case, the mode structure has been inspected in Fig. 2. The corresponding resonance profiles for different toroidal numbers are shown in Fig. 4, showing that, co-passing fast ions have flatter resonance than counter-passing ones. For $n = 2$ case, co-passing fast ions have an extremely flat profile for inner values of the radius, so that the resonance width is much larger than the mode width for all the considered growth rate. For the counter-passing fast ions, the radial resonance profile is steeper, so that the resonance width for low growth rate is smaller than the mode width. As the growth rate increases, a transition from resonance detuning to radial decoupling is expected. For the $n = 3$ and $n = 4$ cases, the resonance frequency radial profile has a larger gradient in the region around the mode localisation.

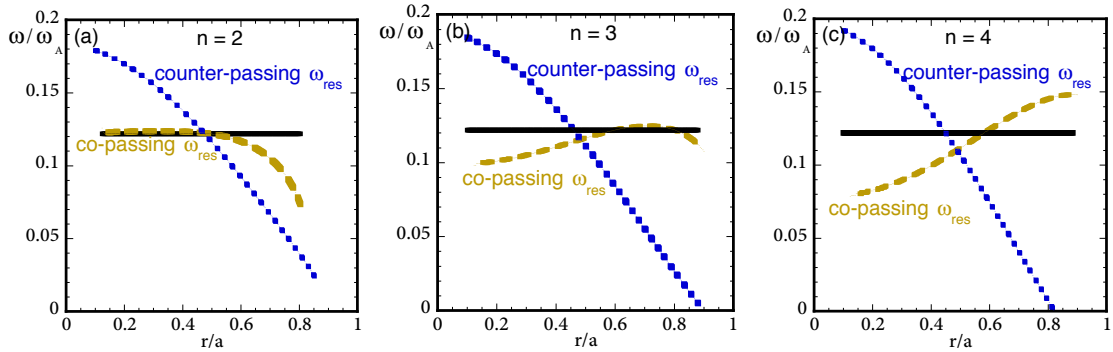

FIG. 4: Radial profiles of different terms contributing to the resonance frequency, for co-passing (top) and counter-passing (centre) fast ions, at different values of the toroidal mode number. Bottom frames show the resulting resonance frequency for both species. The mode frequency is also shown in each frame (solid line).

Figure 5 compares the values of the resonance width obtained from Eq. 4 as the

following:

$$|\omega - \omega_{\rm res}(r_{\rm res} \pm \Delta r_{\rm res}/2)| \simeq \gamma_L, \tag{4}$$

with the measured values of the mode width at different toroidal numbers. We observe

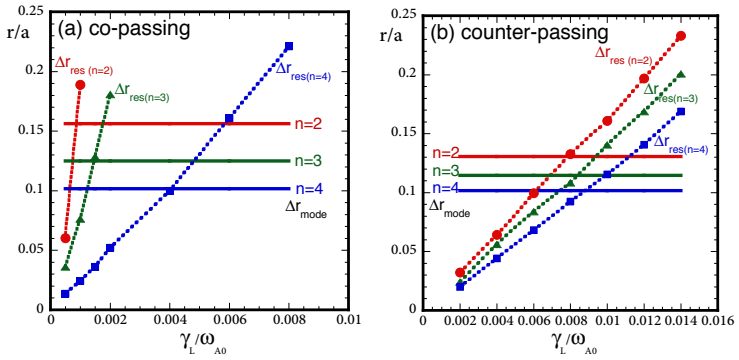

FIG. 5: Resonance width computed by Eq. 4, compared with the measured mode radial width, at different toroidal numbers, for co-passing (left) and counter-passing (right) fast ions.

that, while no relevant difference is obtained for the transition saturation amplitude, the transition growth rate for the counter-passing fast ion case exhibits a weak positive n dependence. Both these results appear to be in better agreement with the results reported in Fig. 3.

3 Energetic particle modes.

We analyse EPM saturation and the corresponding frequency chirping observed both in experiments and simulations (e.g. chirping electron-fishbone by XHMGC simulation [11]). Phase locking has been proposed, within fishbone paradigm [1,6], to describe such chirping: the resonance condition with linearly resonant particles is maintained, while particles are radially displaced, through a continuous modification of the mode frequency. We show that an additional scenario is possible: mode radial localization and frequency appear to be locked to the shear Alfvén continuum; once the linear resonance population has exhausted its driving capability (because of local flattening of the phase-space distribution function), the mode is shifted to non-exhausted regions of the phase space. The effect is a succession of resonant excitations from different phase-space regions (each characterized by its own nonlinear evolution time), rather than mode adjustment to the evolution of the linearly-resonant particles.

The mode is driven unstable on the SAW continuum as shown in Fig. 6. The mode is excited at $\omega_0/\omega_{A0} \simeq 0.19$ where $\omega_{A0} = V_{A0}/R$ is the Alfvén frequency, and the linear growth rate is $\gamma_L/\omega_{A0} \simeq 0.0097$. As the mode is nonlinearly evolved, the mode saturates at $|e\phi/T_H| \sim 10^{-3}$, where ϕ is the perturbed electrostatic potential. After saturation at around $t\omega_{A0} \simeq 650$, the mode amplitude exhibits oscillations. The mode frequency mainly chirps down by about 20% of the birth frequency in around a thousand Alfvén time scale.

In the linear phase, the mode frequency matches the slice of test particles with higher resonance frequency as shown in Fig. 6(a). In the later nonlinear phase, the particle orbits are perturbed, however, the particles are still essentially moving along the line of the perturbed resonance frequency. When the particles lose energy, they move out along the radial direction and their resonace frequencies increase, as shown in the Fig. 6 (b). Meanwhile, the mode frequency chirps down, matching another slice of test particles with lower resonance frequency. In this case, the mode lose contact with the particles driving the mode initially and starts gaining energy from different portion of particles.

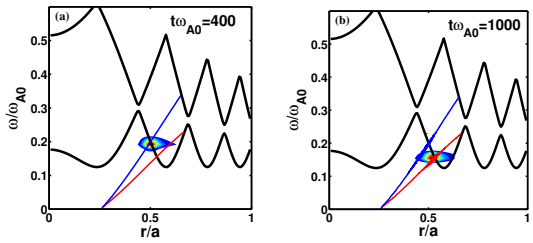

FIG. 6: Two slices of test particle samples are taken with comparison of mode frequency. The line is corresponding to the instantaneous resonance frequency radial profile at (a) $t\omega_{A0} = 400$ and (b) $t\omega_{A0} = 1000$ respectively.

On the other hand, we investigate the power exchange between particles and the mode for each slice of test particle samples, as shown in Fig. 7. When the mode is born, the slice of test particles with higher frequencies are expected to interact with the mode. The power exchange is dominant by those particles. When the mode frequency chirps down, another slice of test particles take part in and start interacting with the mode, the power exchange becomes dominant in the later nonlinear phase.

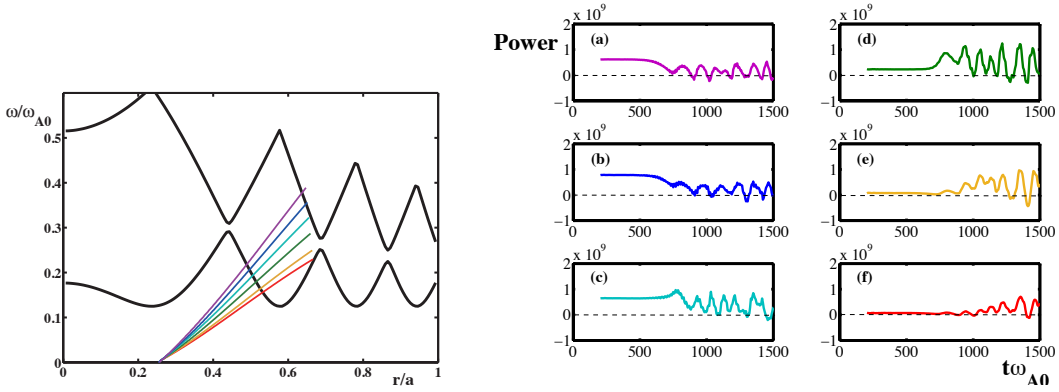

FIG. 7: Time evolution of the power exchange (as shown in the right figure) for each slice of test particles. The color is corresponding to the test particle samples with the same color as shown in the left figure.

4 Acknowledgement

This work has been carried out within the framework of the EUROfusion Consortium and has received funding from the Euratom research and training programme 2014-2018 under grant agreement No 633053. The views and opinions expressed herein do not necessarily reflect those of the European Commission.

References

[1] CHEN L. and ZONCA F. , Physics of Alfvén waves and energetic particles in burning plasmas, Rev. Mod. Phys. 88 015008 (2016).

[2] CHEN L. and ZONCA F., On nonlinear physics of shear Alfvén waves, Physics of Plasmas, Phys. Plasmas 20, 055402 (2013).

[3] CHENG C.Z., CHEN L. and CHANGCE M.S., High-n ideal and resistive shear Alfvén waves in tokamaks, Ann. Phys. 161 21 (1985).

[4] BERK H.L. and BREIZMAN B.N., Saturation of a single mode driven by an energetic injected beam. III. Alfvén wave problem, Phys. Fluids B 2 2246 (1990).

[5] CHEN L., Theory of magnetohydrodynamic instabilities excited by energetic particles in tokamaks, Phys. Plasmas 1 1519 (1994).

[6] ZONCA F. et al., Nonlinear dynamics of phase space zonal structures and energetic particle physics in fusion plasmas, New J. Phys. 17, 013052 (2015).

[7] BRIGUGLIO S. et al., Hybrid Magnetohydrodynamic- Gyrokinetic Simulation of Toroidal Alfvén Eigenmodes, Phys. Plasmas 2, 3711 (1995).

[8] WANG X. et al., An extended hybrid magnetohydrodynamics gyrokinetic model for numerical simulation of shear Alfvén waves in burning plasmas, Phys. Plasmas 18, 052504 (2011).

[9] BRIGUGLIO S. et al., Analysis of the nonlinear behavior of shear-Alfvén modes in Tokamaks based on Hamiltonian mapping techniques, Phy. Plasmas 21, 112301 (2014).

[10] WANG X. et al., Structure of wave-particle resonances and Alfvén mode saturation, Phys. Plasmas 23, 012514 (2016).

[11] VLAD G. et al., Electron fishbone simulations in tokamak equilibria using XHMGC, Nucl. Fusion 53, 083008 (2013).